Coastal wetlands as recorders of earthquake subsidence in the Aegean: a case study of the 1894 Gulf of Atalanti earthquakes, central Greece

A.B. Cundy[a,*], S. Kortekaas[b], T. Dewez[c], I.S. Stewart[c], P.E.F. Collins[c], I.W. Croudace[a], H. Maroukian[d], D. Papanastassiou[e], P. Gaki-Papanastassiou[d], K. Pavlopoulos[d], A. Dawson[b]

[a]School of Ocean and Earth Science, Southampton Oceanography Centre, Southampton SO14 3ZH, UK
[b]Centre for Quaternary Science, William Morris Building, Coventry University, Coventry, UK
[c]Neotectonics Research Centre, Department of Geography and Earth Sciences, Brunel University, Uxbridge UB8 3PH, UK
[d]Department of Geography±Climatology, University of Athens, Gr 15784 Athens, Greece
[e]Institute of Geodynamics, National Observatory of Athens, Gr 11810 Athens, Greece

Abstract

Earthquakes may have a major impact on the morphology and evolution of coasts in tectonically active areas. In the area of the Gulf of Atalanti, central Greece, a damaging earthquake sequence in 1894 is reported to have caused nearshore slumping, tsunami-induced Øooding, and decimetre-to metre-scale coastal subsidence. The earthquakes caused major changes to coastal conÆguration, in particular the separation of the Gaϊduronisi peninsula from the mainland.

Detailed stratigraphical, microfossil and radiometric (^{210}Pb and ^{137}Cs) analyses of coastal wetlands around the Gulf of Atalanti show that these environments preserve evidence of sudden, lasting subsidence contemporaneous with the 1894 events, with foraminiferal assemblages at a site on the mainland opposite the island indicating an abrupt change from supratidal soil to intertidal marine conditions. The elevation change indicated by this terrestrial to marine transition is 30±80 cm. The coastal stratigraphy in the Atalanti area however lacks laterally extensive sharp soil±mud contacts or tsunami deposits of the type used in identifying past earthquake subsidence events at plate±boundary settings. Despite the major earthquake-induced changes in coastal conÆguration, the stratigraphical signature of the 1894 earthquakes is relatively subtle, and is consequently difÆcult to distinguish from other rapid coastal changes (e.g. storm events or barrier breaching) without high-resolution dating control and reference to documentary records. For this reason, coastal wetland stratigraphies are only likely to be useful in identifying pre-historical or poorly documented earthquakes in the Aegean at sites where metre-scale coseismic elevation changes and/or major tsunami inundation have occurred. In addition, the resolution of the biostratigraphic data reported here is insufÆcient to distinguish between the contrasting fault rupture models for the 1894 events. The coastal elevation changes recorded in these wetlands, however, are best accounted for by a slip of 1 m on a multi-segment fault. q 2000 Elsevier Science B.V. All rights reserved.

Keywords: Salt marshes; Earthquakes; Central Greece; Coseismic subsidence; Foraminifera; ^{210}Pb and ^{137}Cs dating; Tectonic models

---

* Corresponding author.

1. Introduction

Earthquakes may have a major impact on the morphology and evolution of coastlines by inducing abrupt coseismic elevation changes (uplift and/or subsidence), extensive shoreline slumping, and transient flooding by tsunami. Following an earthquake, postseismic crustal movements may further influence a shoreline adjusting to a different coastal configuration. Salt marshes and coastal wetlands are particularly sensitive to coseismic and postseismic crustal movements, due to the close relationship between marsh/wetland elevation and local sea level (e.g. Gehrels and Letherman, 1980, and references therein). Sea-level rise or fall induces changes in sedimentation rate and flooding frequency, which may be reflected by changes in lithology and in macro/microfossil assemblages (see Nelson, 1996b for review). This sensitivity to sea-level change has led to a number of studies which have used wetland stratigraphies along tectonically active plate–boundary coastlines as indicators of past large-magnitude ($M > 8$) earthquakes (e.g. Clague and Bobrowsky, 1994; Darienzo et al., 1994; Long and Shennan, 1994; Mathewes and Clague, 1994; Atwater et al., 1995; Hemphill-Haley, 1995; Nelson et al., 1996a,b; Shennan et al., 1996, 1998; Kelsey et al., 1998). These studies have typically used detailed lithological studies and macro- or micro-fossil analyses of coastal sedimentary sequences to identify the timing of past major earthquakes, and the magnitude of coseismic and postseismic crustal movements. McNeill et al. (1998), however, have highlighted the need for high-resolution coastal stratigraphical studies in these plate boundary settings to distinguish local coastal subsidence produced by moderate-magnitude ($M < 8$) earthquakes on local reverse faults from that caused by regional submergence during great earthquakes on the subduction zone. Moderate-magnitude earthquakes also affect many tectonically active coastlines away from plate boundaries. An important question, therefore, is can this stratigraphical approach detect past moderate-magnitude earthquakes in the coastal record of less active tectonic settings?

Along the coastlines of the Aegean Sea, moderate-magnitude (typically $M < 7$) earthquakes are localised on normal faults that bound gulfs or offshore escarpments (Roberts and Jackson, 1988). Here, many coastal wetlands occupy the tectonically subsiding block (hangingwall) of bounding faults, and areas closest to the faults experience significant subsidence during surface faulting. Re-surveying of coastal installations (harbours, mooring points etc.) following the Ms 6.4–6.7 1981 Gulf of Corinth earthquakes (central Greece) showed that parts of the coastline had subsided by as much as 1 m (Hubert et al., 1996). Integrating historical accounts with subsurface archaeological evidence, Soter (1998) argues for up to 3 m of subsidence associated with the 373 BC earthquake (M 6.8 — Papazachos and Papazachou, 1997) along the Helike Fault in the western Gulf of Corinth. These estimates of metre-scale subsidence suggest that earthquake effects ought to be readily detectable in the stratigraphy of coastal lowlands, particularly as most of the circum-Aegean coastline is microtidal (mean tidal range of less than 0.5 m). Here we examine whether coastal wetland stratigraphies can be used to reconstruct the coastal changes caused by a well-documented moderate-magnitude earthquake sequence in central Greece — the 1894 Gulf of Atalanti earthquakes.

2. Coastal changes during the 1894 Atalanti earthquake sequence

The Gulf of Atalanti area (Fig. 1) experienced major coastal changes during an earthquake sequence in 1894, a sequence dominated by a $M = 6.2$ event on 20th April and a $M = 6.9$ event on 27th April (Ambraseys and Jackson, 1990). Contemporary accounts of earthquake damage (Skuphos, 1894; Papavasiliou, 1894; Mitsopoulos, 1895) attribute extensive coastal slumping and liquefaction to the 20th April ($M = 6.2$) event, and surface faulting, coastal subsidence and tsunami inundation to the 27th April ($M = 6.9$) event. While documentary accounts provide useful information on the main impacts of the earthquakes, the accounts are often contradictory when describing the extent of marine flooding and the amount of coseismic subsidence induced.

Coastal subsidence was reported to result from three main processes: localised slumping, liquefaction, and
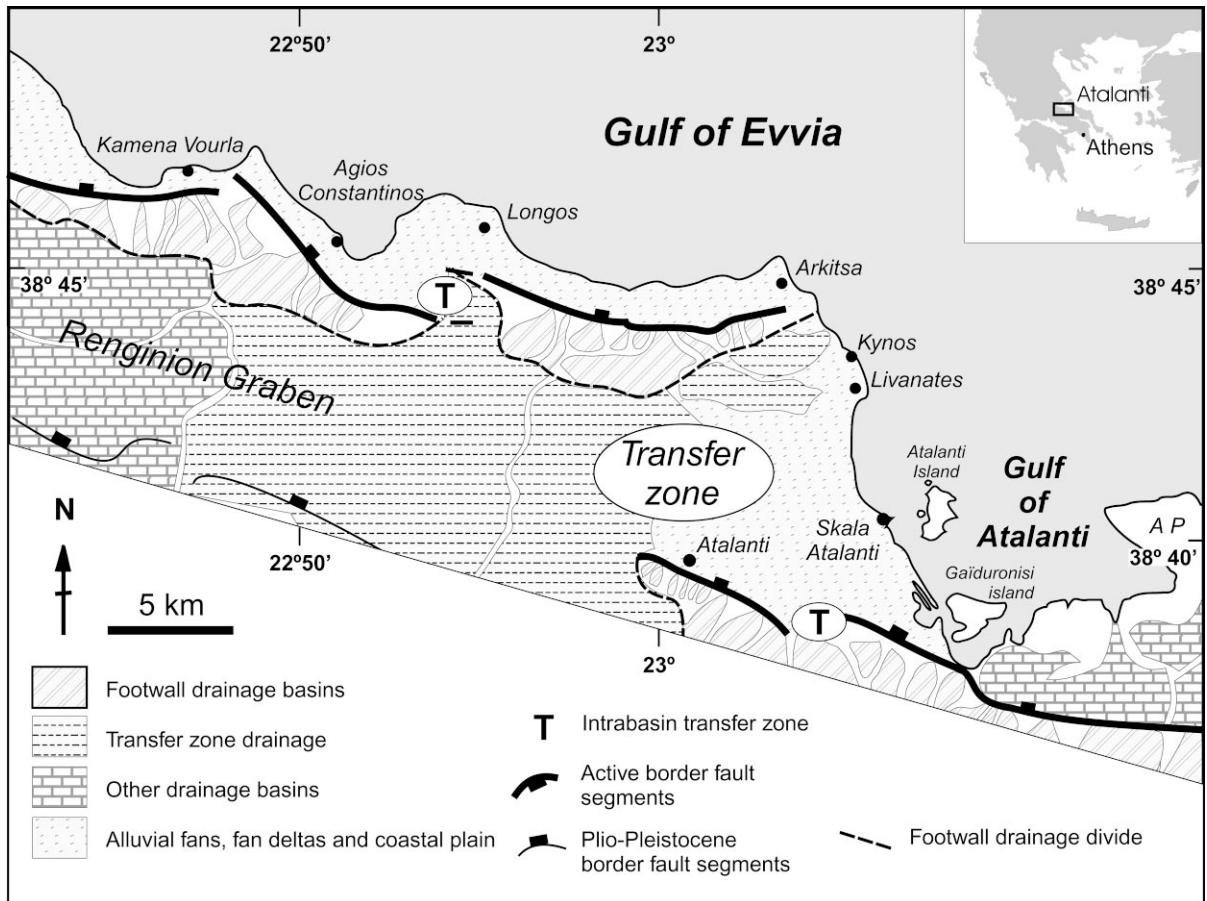
Fig. 1. Simplified tectonic and drainage setting of the Gulf of Atalanti, showing the position of the Atalanti coastal plain in the transfer zone between the major normal faults of Atalanti and Kamena Vourla (after Gawthorpe and Hurst, 1993). AP; Aetolymion Peninsula. Inset map shows the location of the Gulf of Atalanti area in Greece.

broader tectonic downwarping. The 20th April event caused extensive liquefaction and slumping along the coastal plain between Almyra and Livanates (Ambraseys and Jackson, 1990). For example, the stone harbour at Kato Peli (now Skala Atalanti) is reported in contemporary telegram transmissions (Akropolis newspaper, 1894) as having split and its southern causeway subsided into the sea. The remains of this causeway are found in the modern harbour at approximately 2 m below the present high water mark. There is no evidence, however, for widespread marine inundation of the Atalanti coastal zone during the 20th April earthquake.

The coastal effects of the 27th April event were far more dramatic:

this second jolt was, from more than one point of view remarkable. Thus, at the time of the jolt, the sea, on all the extent of the coast, from the Bay of St. Theologos (on the west of the peninsula of Aetolymion) as far as the village of St. Constantin, a wave submerged the coast for a distance of some tens of metres in general. The sea has withdrawn to its initial place, except in the Plain of Atalante, of which the most part of the coast, that in the north, remained covered by water for a distance of some metres, while the

southern part plunges in water for a distance of some tens of metres. This immersion, after which the peninsula of Gaïduronisi, at the far end of the Bay of Atalante, was transformed into an island, is due to a subsidence of that plain…Papavasiliou (1894).

From this and other contemporary reports (Skuphos, 1894; Mitsopoulos, 1895), coastal flooding accompanying the 27 April earthquake appears to have been caused by tsunami inundation superimposed upon broad tectonic subsidence. That the flooding between Aghios Konstantinos and the Aetolymion peninsula was a tsunami is suggested by eye-witness accounts at Almyra, Kato Peli and Agios Constantinos, which reported that the sea initially withdrew several tens of metres then abruptly returned as a giant wave (Skuphos, 1894). The coastal zone between Almyra and Kato Peli, however, remained flooded after the retreat of the tsunami, though estimates of the extent of inundation in this area vary. Skuphos (1894) reported a 300-m-wide inundation zone between Almyra and Kato Peli. Papavasiliou's description (above) of greatest inundation in the south, however, supports the observation by Mitsopoulos (1895) that in the north (between Palaeomagasa and Kato Peli) only a narrow strip of land (10–20 m) was inundated. Both Skuphos and Mitsopoulos agree, however, that permanent inundation did not extend north of Kato Peli.

Both Papavasiliou (1894) and Skuphos (1894) state that the observed 'permanent' coastal inundation in the southern part of the Atalanti plain was consistent with tectonic subsidence induced by movement on the coast-bounding Atalanti Fault. These authors also noted the detachment of the Gaïduronisi peninsula from the mainland as supporting evidence for this subsidence. This permanent separation is obvious in a comparison of the pre-earthquake British Admiralty chart of 1890 with aerial photographs taken in 1945 and 1986 (Fig. 3).

Estimates of the magnitude of coastal subsidence caused by the earthquake vary. In particular, the 25–30 cm of submergence recorded in the Almyra area by Skuphos (1894) contrasts with Papavasiliou's contention that "the whole region of Atalanti got separated

from the Roda Mountain and sank for about 1.5 m" (Akropolis newspaper, 1894). Hence, the eyewitness accounts are ambiguous in terms of constraining both the extent and the magnitude of coastal subsidence accompanying the 1894 earthquakes.

Modern reappraisals of the contemporary accounts of the 1894 Atalanti earthquakes, some augmented by recent field mapping, continue the disagreement about the magnitude and extent of earthquake deformation accompanying the main (27 April) seismic shock. Following Skuphos (1894), some workers accept that the Atalanti (or Lochris) Fault ruptured over its full length, a distance of 50–60 km (e.g. Karnik, 1968; Lemeille, 1977; Stiros and Rondoyianni, 1985; Stiros, 1986). According to Papazachos and Papazachou (1997), the 55-km-long rupture was associated with a general subsidence of the hangingwall by 1–1.5 m. These authors consequently ascribe a magnitude of M 7.2 to this event. In contrast, Ambraseys and Jackson (1990) distinguish a 25-km-long zone (Martino-Atalanti) of primary ground rupture, along which fault displacements are around 1 m, from a 15-km-long zone of faulting northwest of Atalanti where fault displacements are only a few tens of centimetres. On the basis of a smaller total rupture length (40 km) and 0.5 m of coastal subsidence between Arkitsa and Almyra, they derive a magnitude estimate of Ms 6.9 (Ambraseys and Jackson, 1998). Ganas et al. (1998) and Pavlides et al. (1998) associate the 27 April event only with the primary rupture zone east of Atalanti, (the 'Atalanti Fault Segment' of Ganas et al. (1998)), and derive total rupture lengths of 30 and 34 km, respectively. Although Pavlides et al. (1998) discriminate between an average fault displacement of 0.25 m in bedrock and up to 1.5 m displacement in superficial deposits (cf. Skuphos, 1894; Stiros and Rondoyianni, 1985) they also estimate the magnitude as Ms 6.9.

These different rupture length/fault displacement scenarios reflect both the ambiguity of the contemporary reports and the absence of ground breaks that can be unequivocally associated with the 1894 events (Ambraseys and Jackson, 1990). An independent evaluation of the competing rupture scenarios would be valuable because the fault parameters derived from

these scenarios are directly or indirectly used in seis-mic-hazard assessments. Hence, this study examines the extent to which high-resolution stratigraphical investigations of the wetlands in the Almyra to Skala Atalanti coastal strip can be used to identify and constrain the coastal subsidence caused by the 1894 earthquake events.

3. Methods

The Atalanti wetlands are confined to the coastal zone between Tragana and Skala Atalanti, immediately seaward of the Atalanti Fault (Fig. 2). This zone consists mainly of sandy beaches enclosing shallow marshy lagoons or, in more sheltered areas closer to the fault, narrow fringing salt marshes (Plate 1). Previous investigation of the Holocene stratigraphy in the Atalanti coastal plain (based on 30-m-deep boreholes from the area around Tragana) records an alternating sequence of mainly fluvial silt, sand and conglomerate. An uppermost 1-m-thick mud unit caps a 3-m-thick deposit of ophiolitic conglomerate interbedded with silty clays (Rondoyianni-Tsiambaou, 1984).

In this study, the near-surface stratigraphy of coastal wetlands between Almyra and Skala Atalanti (Fig. 2) was investigated with over fifty 1- to 2-m-deep cores, each taken with a 6-cm-wide, 1-m-long hand-driven gouge corer. The cores were logged and subdivided into continuous 1- or 2-cm-thick depth increments. The elevations of all coring sites were determined using a Zeiss Autoset level or a Sokkisha total station. All levelling traverses were closed with errors less than or equal to 0.05 m. In the absence of a reliable elevation benchmark or local tide gauge, all
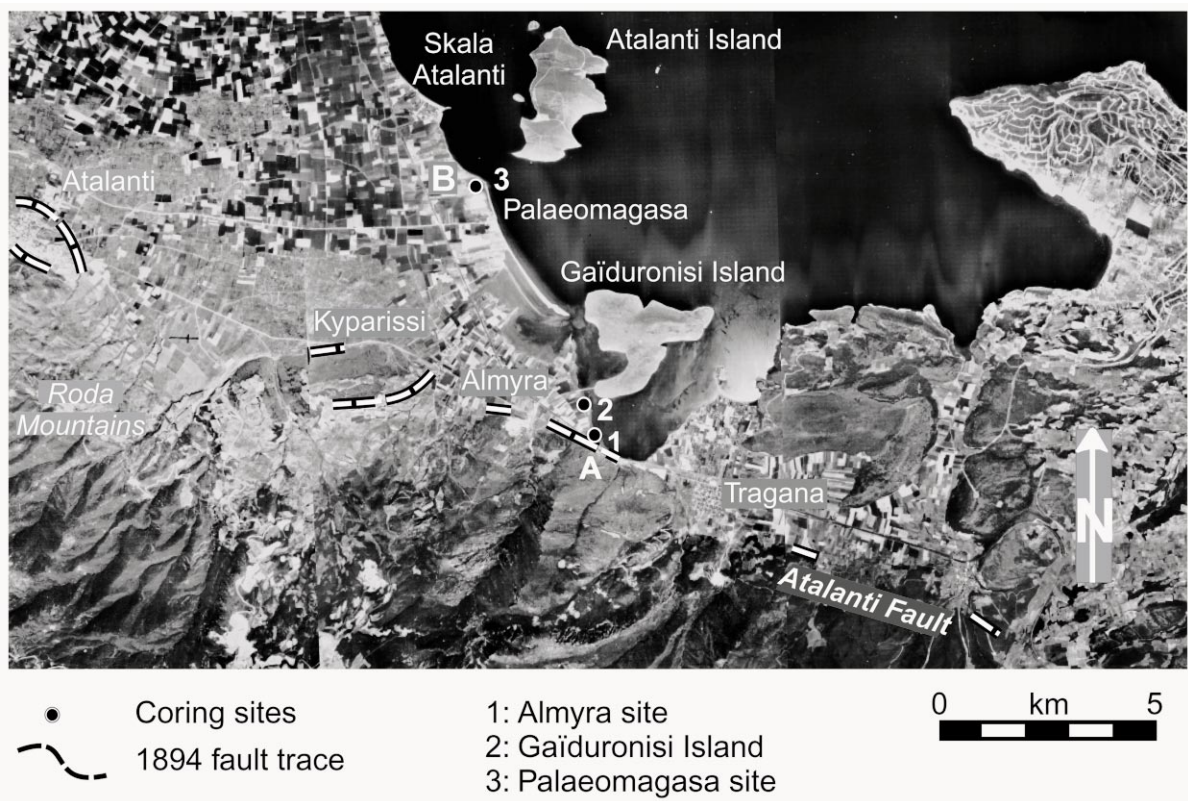

Fig. 2. Study area, the Gulf of Atalanti. The Atalanti Fault is shown by the white dashed line. Numbered black circles show coring locations referred to in the text. Note that the embayment to the north-west of Gaïduronisi island is partially enclosed by two spits. The landward of the two is a narrow (ca. 5 m wide) strip of salt marsh that is probably the vegetated embankment of a former salt-manufacturing area or fishery.
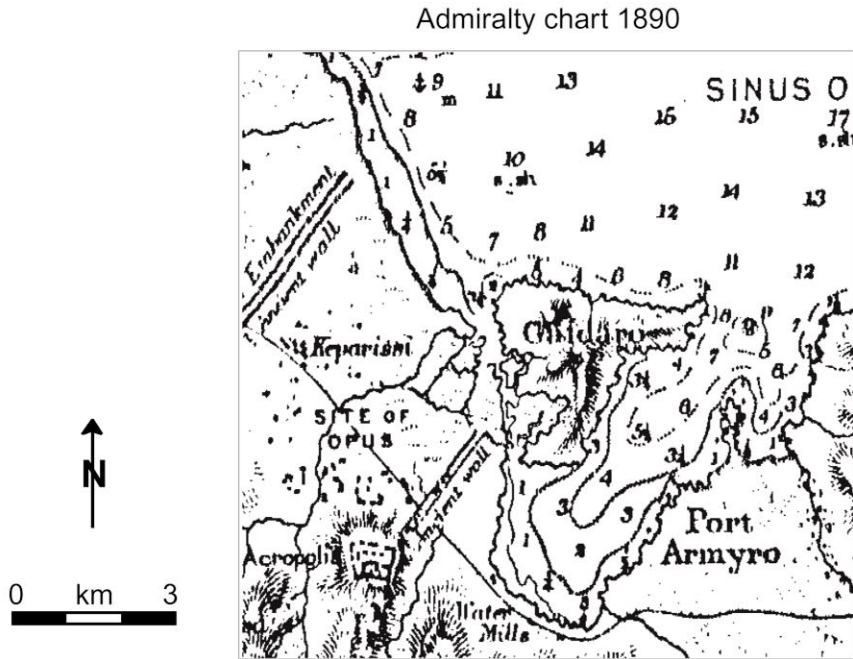
Fig. 3. British Admiralty Chart of 1890 and aerial photographs from 1945 and 1986, central Gulf of Atalanti. Depths shown on the British Admiralty chart are in fathoms (1 fathom = 1.829 m). The 1890 chart shows that prior to the earthquake the area between Gaïduronisi island and the mainland was an area of low-lying marsh bisected by a small creek, whereas the modern coastline shows a 300 m wide marine channel separating the island from the mainland. An extensive shallow embayment northwest of the island was flooded between 1890 and 1945, probably as a result of earthquake-induced barrier-breaching and flooding of former salt-workings or enclosed fisheries.

Plate 1. View towards the south-east showing narrow fringing salt marshes between Gaïduronisi island and Almyra, in the southern Gulf of Atalanti. In the background is the escarpment of the Atalanti Fault (Martinon segment). The 1894 earthquake ruptured along the base of this escarpment, causing widespread subsidence of the coastal zone.

elevations are reported relative to the elevation of the maximum high water tide at Palaeomagasa (Fig. 2) in September 1998. The mean spring tidal range in the area is 60–70 cm, as determined by total station measurements of sea-level fluctuations during June 1999 and as reported to us by the Skala Port Authority.

^{210}Pb and ^{137}Cs dating was carried out on selected core samples. ^{210}Pb (half-life = 22.3 years) is a naturally produced radionuclide that has been extensively used in the dating of recent sediments. Dating is based on determination of the vertical distribution of ^{210}Pb derived from atmospheric fallout (termed unsupported ^{210}Pb, or ^{210}Pb$_{excess}$), and the known decay rate of ^{210}Pb (see Appleby and Oldfield, 1992 for further details of the ^{210}Pb method). ^{210}Pb activity was determined by a proxy method through alpha spectrometric measurement of its grand daughter nuclide ^{210}Po. The method employed is based on Flynn (1968), using double acid leaching of the sedi-

ment with ^{209}Po as an isotopic tracer and autodeposition of the Po isotopes in the leachate on to silver discs. Detection limits are 0.1 Bq/kg. The ^{210}Pb$_{excess}$ activity was estimated by subtraction of the value of constant ^{210}Pb activity at depth (0.013–0.017 Bq/g). Sediments were dated in this study using the CRS (Constant Rate of Supply) model of ^{210}Pb dating (Goldberg, 1963).

^{137}Cs (half-life = 30 years) is an artificially produced radionuclide, present in the environment due to atmospheric fallout from nuclear weapons testing and reactor accidents, and from discharges from nuclear facilities. Global dispersion and fallout of ^{137}Cs occurred from 1954 onwards following the detonation of high-yield thermonuclear weapons. Distinct maxima in fallout occurred in 1958 and 1963 (from nuclear weapons testing) and in the northern hemisphere in 1986 (from the Chernobyl incident). In favourable conditions, these periods of peak fallout/discharge provide subsurface activity maxima

in accumulating sediments, which can be used to derive rates of sediment accretion (e.g. Ritchie and McHenry, 1990; Cundy and Croudace, 1996; Cundy et al., 1998). [137]Cs activities were determined by gamma spectrometry with a Canberra 30% P-type HPGe detector. Errors were typically in the order of 4% (1σ), and detection limits are 0.5 Bq/kg.

Sediment samples were also analysed for foraminiferal tests. Foraminiferal assemblages in salt marshes vary with elevation, and the comparison of the modern distribution of marsh foraminifera with fossil assemblages from a sediment core can be used to interpret past changes in relative sea level (e.g. Scott and Medioli, 1978). Consequently, marsh foraminifera have been used to estimate the amount of earthquake-induced subsidence in a number of studies at the Cascadia subduction zone (Clague and Bobrowsky, 1994; Guilbault et al., 1995; Nelson et al., 1996b; Shennan et al., 1996). Samples for foraminiferal analysis were washed over a 63 μm sieve. Organic-rich samples were counted wet because these sediments tend to form a solid organic crust when dried; all other samples were counted dry. Three different samples were counted dry as well as wet to examine whether agglutinated species were lost in the drying process, but no significant difference was found between wet and dry counts. The two agglutinated species found in these samples, *Trochammina inflata* and *Jadammina macrescens* seemed to withstand drying, and although the chambers in the tests of *J. macrescens* often collapsed when dried, they were still identifiable. Organic-rich samples were stored in water and divided into subsamples with a wet splitter prior to counting. The other samples were oven-dried at 40°C and counted using a dry sample splitter. At least 300 foraminifera were counted for each sample. Fragments of broken foraminiferal test were only counted if they were large enough to be identified and only if the fragment contained the umbilicus (to prevent counting the same specimen twice). Foraminiferal species identification was made with reference to Cimerman and Langer (1991) and the Challenger Foraminifera Atlas (Jones, 1994). Modern surface salt-marsh samples were collected along a transect close to the Gaïduronisi site (see below) which covered a vertical range of 12 cm (−2 to +10 cm above MHW). No significant differences were found between foraminiferal assemblages from the different

samples, except the sample taken from the seaward edge of the marsh (just above the intertidal mudflat) which contained many mudflat and shallow-marine calcareous species. In all other marsh samples two agglutinated species were found: *J. macrescens* (82–94% of total assemblage) and *T. inflata* (6–18% of total assemblage), indicative of a high marsh environment (Scott et al., 1979). Because little zonation in foraminiferal assemblages was found in this marsh transect, the assemblages are not used as sea-level indicators in this study. Instead, they are only used as general palaeoenvironmental indicators, i.e salt marsh, intertidal mudflat or shallow marine.

Preliminary pollen analyses were carried out on selected samples. Samples were prepared using standard techniques (cf. Moore et al., 1991) with NaOH, HCl, HF and acetolysis treatments. Prepared samples were mounted in glycerine, with a safranin stain. Slides were examined at 400 × magnification, with 1000 × and phase contrast used for problematic grains. Identification was made with reference to type slides (Moore et al., 1991) where necessary. Pollen nomenclature principally follows Moore et al. (1991), modified to take into account the comments of Bennett et al. (1994).

4. Sedimentary records of recent environmental change in the Atalanti wetlands

The near-surface (ca. −2 m to surface) stratigraphy of the Atalanti wetlands is extremely heterogeneous (Fig. 4). In general, ophiolitic grit and gravel is overlain by 1–2 m of clay interbedded with sand and silt units. The organic-rich silty clay of the present-day salt marshes forms a thin (5- to 30-cm-thick) veneer at the surface. All cores show sharp contacts between sedimentary units, indicating rapid changes in depositional conditions or intervening periods of erosion. Three sites are discussed in detail — one within 200 m of the Atalanti Fault (Almyra), one 600 m from the fault and immediately landward of Gaïduronisi island (Gaïduronisi), and one 3 km from the fault (Palaeomagasa) (Figs. 2 and 4).

4.1. Almyra site

The Almyra site is adjacent to the Atalanti Fault in the area of maximum post-earthquake inundation

Fig. 4. Surface stratigraphy of Atalanti wetlands from south to north along the transect (A)–(B) (see Fig. 2 for location of transect). All elevations shown are relative to maximum high water level at Palaeomagasa for September 1998. Cores analysed for foraminifera and radiometrically dated are marked 1 (Almyra), 2 (Gaïduronisi) and 3 (Palaeomagasa).

reported by contemporary sources. The site consists of salt marshes fringing low-lying agricultural land.

4.1.1. Stratigraphy

The salt-marsh core shows a shallow (3 m) stratigraphy of coarse sands with grits, overlain by a grey–black clay, which is in turn overlain by coarse and fine sands that grade into an organic-rich silty clay (the present-day salt marsh surface sediments) (Fig. 5). The coarse sand and grits below −35 cm presumably correspond to the near-surface ophiolitic conglomeratic deposits described by Rondoyianni-Tsiambaou (1984). The sharp contact that marks the change from sand and grit to clay deposition at −35 cm suggests either a sudden change in depositional environment or erosion. The clay-rich unit from −11.5 to −35 cm contains foraminifera indicative of intertidal mudflat and shallow marine environments (Fig. 5). The contact between the shallow sands below +2 cm and the clay unit at −11.5 cm is extremely sharp and well defined. The lowest part of the sand unit shows an increase in some shallow marine taxa (e.g. *Elphidium* spp., *A. beccarii* var. batavus), grading into species characteristic of lower intertidal environments (*A. beccarii* and *H. germanica*). The sequence then grades into silty clay containing *T. inflata* and *J. macrescens* (+2 cm to surface), representing the modern salt-marsh environment.

4.1.2. Radiometric dating

^{210}Pb dating of the upper stratigraphy (Fig. 5) indicates that the clays at −35 cm to −11.5 cm are older than ca. 100 years. ^{210}Pb in this unit has activities only slightly greater than the supported activity of 0.013–0.017 Bq/g, indicating that the sediment is sufficiently old for the ^{210}Pb derived from atmospheric fallout (the excess ^{210}Pb) to have decayed to very low levels. This is usually assumed to take at least 100 years. The sand layer between −11.5 cm and +2 cm depth is not amenable to dating by ^{210}Pb. However, the shallow, organic-rich silty clay (+2 cm to surface) has high ^{210}Pb$_{excess}$ values (0.054–0.107 Bq/g), indicating deposition within the last 30 years (estimated from comparison of activities with the ^{210}Pb$_{excess}$ profile and age-depth curve at the Gaïduronisi island site, see Fig. 6). The lack of a clear decline in ^{210}Pb activity with depth in this unit precludes more accurate dating by the ^{210}Pb method.

4.1.3. Interpretation

The stratigraphy outlined for the Almyra site shows evidence for an abrupt change from silty clay to sand deposition at −11.5 cm, with an increase in the relative percentage of some shallow marine foraminifera at the base of the sand unit. This change is consistent with an abrupt deepening of the depositional environment due to coastal subsidence caused by the 1894 earthquake sequence. However, the lack of accurate dating control means that other abrupt coastal processes, such as storm events or barrier breaching, cannot be discounted (see Section 5). Even if an earthquake mechanism is assumed, no estimate of subsidence can be determined from this sequence because the elevation of the sand unit cannot be precisely related to a former sea level.

4.2. Gaïduronisi island site

The Gaïduronisi site consists of a narrow (∼20 m) salt marsh immediately south of the recently constructed causeway between Gaïduronisi island and the mainland (Fig. 2 and Plate 1). At the seaward edge of the marsh is the basal stonework of a ruined building, possibly a former bath fed from an active freshwater spring that upwells behind the marsh at this point. These ruins are submerged at high tide and are draped landward by intertidal marsh, suggesting that they have subsided relative to sea level since the time of construction. The structure is not listed in the local 'Sites and Monuments' record and its age is not known (E. Zachou, pers. comm.).

4.2.1. Stratigraphy

The stratigraphy at this site (Fig. 6) comprises brown silt with grit clasts below −21 cm, overlain by a thin (3 cm) layer of silty-sand, which is in turn overlain by a prominent unit of laminated white, red and grey fine-grained travertine (−18 to −10 cm). This travertine unit is overlain by grey silt that grades into organic-rich silty clay at the surface.

Foraminiferal analysis shows that the basal brown silt unit (below −21 cm) contains few foraminifera. Those foraminifera that are present are highly abraded. Pollen was sparsely present within this unit, and those grains present were generally poorly preserved. Of the 51.5 grains that were identifiable, only three were well preserved, the rest being
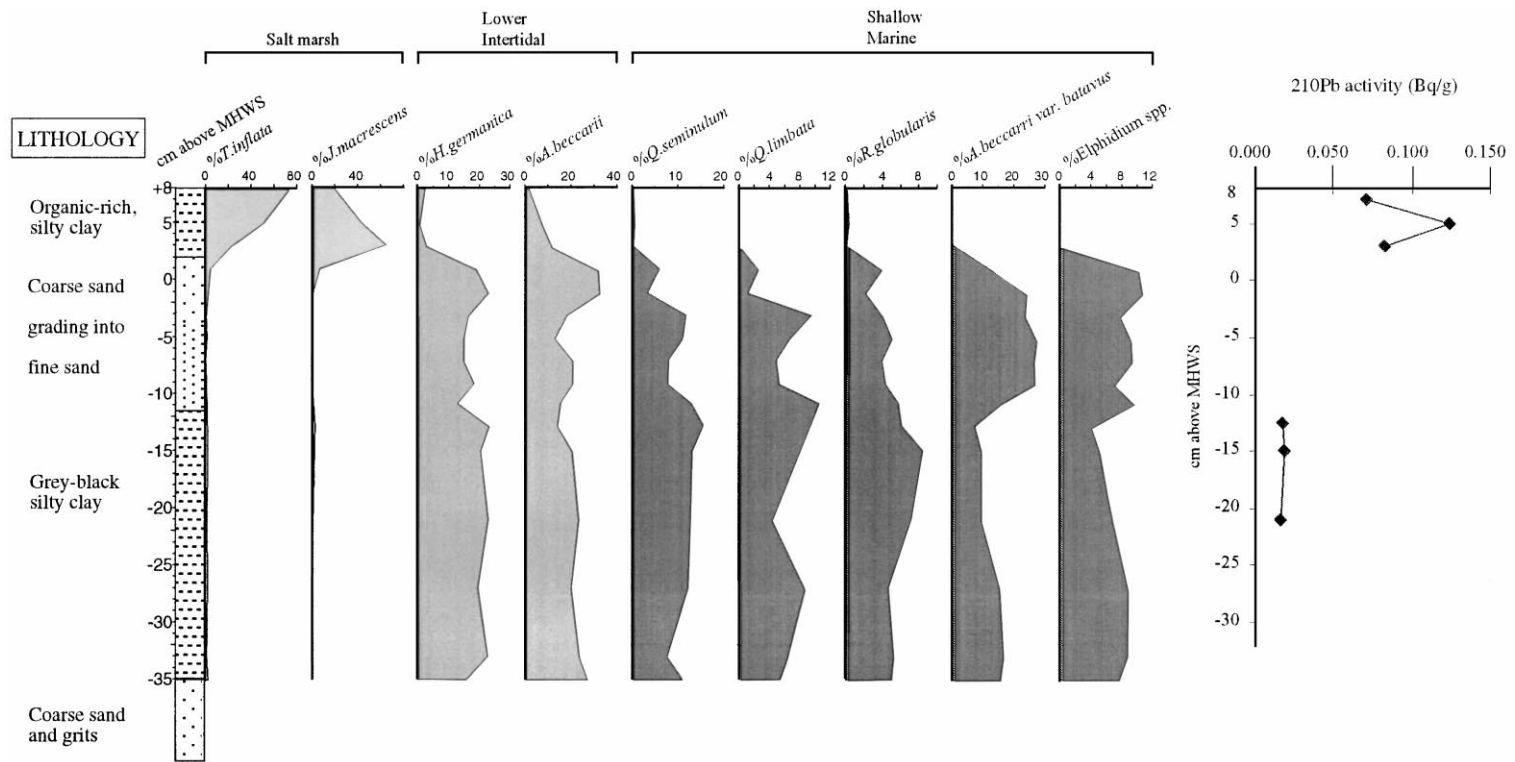
Fig. 5. Foraminiferal abundances (relative percentages) and ^{210}Pb activity vs. depth for the Almyra site (see Fig. 2 for site location). Only foraminifera species which occur with a relative percentage of greater than 5% are plotted.
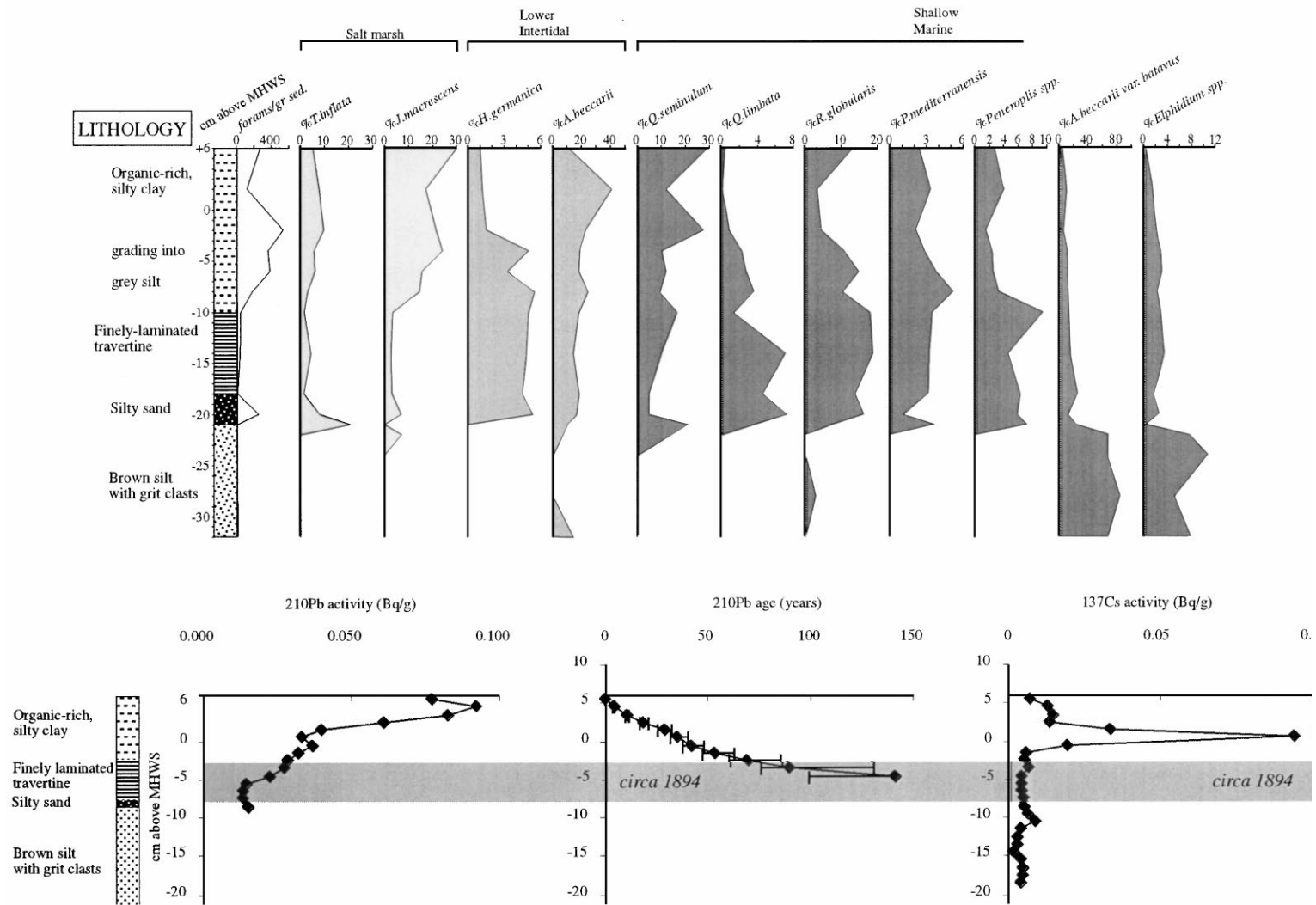
Fig. 6. Foraminiferal abundances (relative percentages) and ^{210}Pb and ^{137}Cs activities vs. depth for the Gaïduronisi site (see Fig. 2 for site location). Only foraminifera species which occur with a relative percentage of greater than 5% are plotted. The age-depth graph shown is derived using the CRS model of ^{210}Pb dating. Errors on the age-depth graph are based on the uncertainty of the ^{210}Pb supported activity (0.015 ± 0.002 Bq/g).

deteriorated in some way. The dominant form of deterioration was crumpling or breaking, indicating mechanical attack. Most of these grains also exhibited other forms of deterioration such as corrosion or breakdown of the exine structure, rendering the grain wall amorphous. The pollen assemblage is dominated by Asteraceae pollen, particularly Lactuceae. This type is resistant to decay and may be significantly over-represented in assemblages extracted from soils or which contain eroded soil material (e.g. Cundy et al., 1998). Chenopodiaceae are only present in low numbers. Although this might be a reflection of differential preservation, it could indicate the absence of salt marsh vegetation from the immediate proximity of the coring site. A key feature of sediment from this basal unit was the abundance of microscopic charcoal fragments, indicating either burning or perhaps dessication and pedogenesis. Either process indicates a terrestrial environment. A terrestrial, rather than marine, setting is also indicated by foraminiferal analyses. The low abundance of foraminifera and their abraded nature is consistent with wind transport of foraminiferal remains from the upper intertidal zone onto a low-lying, supratidal coastal soil.

The overlying silty-sand (−21 to −18 cm) contains a mixture of marsh, intertidal and marine foraminifera. The travertine laminae show a low number of foraminifera, but the species present indicate some marine influence. The mineralogy of the travertine was determined qualitatively by X-ray diffraction and consists of mixed calcite and quartz, with traces of halite and dolomite. There were no significant mineralogical variations between the laminae in the travertine. The mineralogy, the presence of foraminifera and the fine-grained laminated nature of the deposit, indicate settling of precipitated carbonates in a low-energy marine environment. Compared to the basal brown silt unit, pollen was much more frequent and generally better preserved in the travertine unit, reflected by the lower number of grains that could not be identified. Bisaccate, wind-pollinated taxa, dominate, particular pines (at least two species were identifiable) and Abies, and this implies their presence locally. In a coastal setting, however, their high frequency may reflect preferential sorting by water currents or waves. Such a hypothesis is supported by the presence of Chenopodiaceae,

suggesting nearby salt marsh vegetation communities. Significantly, specimens of the foraminifera *Rosalina globularis* found within the travertine and the underlying silty-sand (−21 to −18 cm) have no floating chamber. Growth of a floating chamber is a feature of the reproduction cycle of *R. globularis*, and only occurs in September and October (Donnici et al., 1997). The absence of specimens with a floating chamber indicates therefore that deposition of these units occurred rapidly, i.e. in less than 10 months. The absence of a floating chamber is unlikely to be a preservation effect, as *R. globularis* specimens with floating chambers were found in upper sections of the core from this site (above −10 cm).

The foraminifera in the sediments above the travertine unit (−10 cm to surface) show a gradual transition from shallow marine and intertidal mudflat assemblages to marsh assemblages characteristic of the present-day salt marsh.

4.2.2. Radiometric dating

^{210}Pb dating of a parallel core (Fig. 6) indicates that the travertine unit is broadly contemporaneous with the 1894 earthquakes. The upper sample of the travertine unit has a ^{210}Pb age of 90 years (range = 75–130 years). It is difficult to assess how rapidly the travertine unit was deposited using ^{210}Pb, due to the large errors on the age determination at this depth. The sediments above the travertine unit accreted relatively uniformly up to the present day, at an average rate of 1.2 mm/yr. ^{137}Cs activity shows a strong subsurface activity peak around a depth of −5 cm (Fig. 6). This probably corresponds to the 1963 global fallout maximum from above-ground nuclear weapons testing. The remote position of central Greece in relation to the main track of the Chernobyl ^{137}Cs "plume" (e.g. Smith, 1988) and the rapid drop in activity below the ^{137}Cs maximum implies a weapons testing, rather than a Chernobyl, source. A 35 year ^{137}Cs age agrees well with an estimated age of 32 years (1966) for the same depth from ^{210}Pb dating. Ascribing the ^{137}Cs peak to 1963 gives an average accretion rate of 1.6 mm/year since 1963.

4.2.3. Interpretation

At the Gaïduronisi site, coastal sediments preserve a record of a change from terrestrial to marine sedimentation at −21 cm. Pollen and foraminiferal data,

in combination with ^{210}Pb and ^{137}Cs dating, are consistent with the abrupt submergence of a low-lying terrestrial soil around 1894, the rapid deposition of silts, sands and carbonates in a marine intertidal environment, and a subsequent gradual accretion of sediment to form the present day salt marsh. The silty-sand unit overlying the supratidal soil at −21 cm shows evidence for rapid deposition, and so may have been deposited by the tsunami reported in contemporary accounts. Alternatively, deposition of this unit may be a direct result of marine flooding following coastal subsidence, rather than a tsunami per se.

The carbonate travertine unit, which is dated by ^{210}Pb assay to around the time of the 1894 earthquake, may be a product of the transient expulsion of groundwaters associated with fault rupture, a phenomenon documented to accompany earthquake faulting elsewhere (Muir Wood and King, 1993). Skuphos (1894, p. 441) noted that freshwater springs at Almyra ceased for 60 h immediately after the 27 April mainshock, and thereafter became brackish with a twofold increase in flow. Mitsopoulos (1895, pp. 29–32) reported that groundwater springs at Skala changed colour as a result of "dissolved clays and sands", and that there was a creamy discoloration of the sea between Gaïdaronisi and Almyra. These observations, together with the localised development of travertine at the Gaïdaronisi site, could be explained by a short-lived expulsion of carbonate-rich spring waters, possibly from an active spring that is found a few metres landward of the Gaïdaronisi coring site. If travertine deposition was indeed initiated by the earthquake in late April, then, as explained above, the absence of *R. globularis* with floating chambers in the associated sediments would indicate that deposition had ceased by September–October. This indicates that the 8-cm-thick unit was deposited in a period of 4–5 months.

Assuming that the terrestrial–marine contact at −21 cm was caused by the 1894 earthquakes, the elevation change represented by a terrestrial to marine transition allows an estimate of earthquake-induced subsidence to be made. While the elevation of the supratidal soil surface at −21 cm cannot be accurately related to a former sea-level, the incorporation by this buried soil of abraded, possibly wind-transported foraminifera indicates that its elevation was relatively close to (within 0.5 m) of mean high water spring tide level. Since the tidal range at Gaïduronisi is 60–

70 cm, the maximum subsidence represented by the change from a soil to an intertidal environment is therefore ca. 120 cm. The minimum subsidence which would cause a similar terrestrial to intertidal change is ca. 30 cm (the minimum elevation difference between soil and intertidal muds at the site). Hence, the terrestrial–marine contact at −21 cm indicates earthquake subsidence of 30–120 cm. As the terrestrial–marine contact is only 27 cm below the present high-marsh surface, however, an upper subsidence limit of 120 cm is clearly too high. Instead, based on the elevation difference between the buried soil surface at −21 cm and the contemporary soil immediately behind the high-marsh (around 60 cm above MHWS), we estimate that the upper limit of earthquake-induced subsidence at this site is 80 cm.

4.3. Palaeomagasa site

The Palaeomagasa site consists of a 100-m-wide marsh behind a discontinuous sand and shingle barrier. A few hundred metres to the southeast, at the modern shoreline, partially and fully submerged buildings (possibly Early Byzantine baths, Dakoronia oral comm. 1998) indicate subsidence of this coast, although the period over which subsidence occurred is not known.

4.3.1. Stratigraphy
The stratigraphy at Palaeomagasa (Fig. 7) comprises coarse sand and grits below −20 cm, overlain by fine sand with clay between −20 and 0 cm, which is in turn overlain by organic-rich silty clay from 0 cm to +16 cm. The foraminiferal assemblage in this core between −18 cm and +16 cm shows a gradual transition from marine to lower intertidal to salt marsh species, consistent with gradual accretion of intertidal sediment and salt marsh.

4.3.2. Radiometric dating
[210]Pb dating of the silty clay (Fig. 7) indicates relatively uniform sediment accretion (at approximately 1 mm/y) with the time of the 1894 earthquake corresponding to a depth of 12 cm below the marsh surface (at −4 cm).

4.3.3. Interpretation
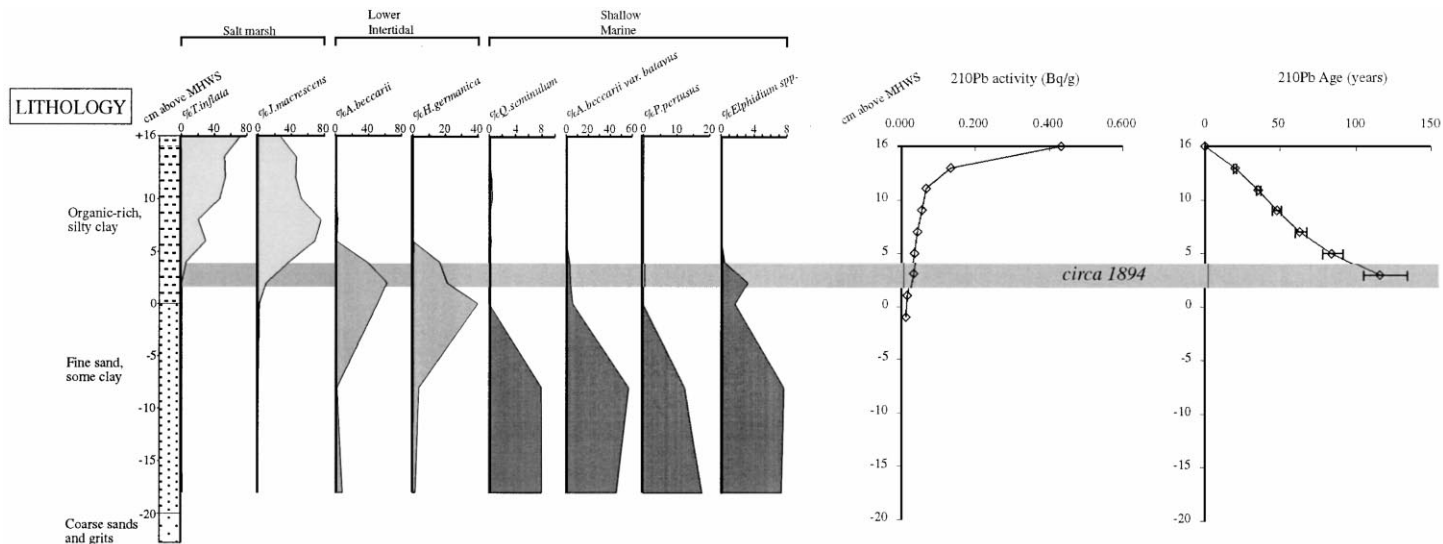In contrast to Almyra and Gaïduronisi, there is no

Fig. 7. Foraminiferal abundances (relative percentages) and ^{210}Pb activity vs. depth for the Palaeomagasa site (see Fig. 2 for site location). Only foraminifera species which occur with a relative percentage of greater than 5% are plotted. The age-depth graph shown is derived using the CRS model of ^{210}Pb dating. Errors on the age-depth graph are based on the uncertainty of the ^{210}Pb$_{supported}$ activity (0.015 ± 0.002 Bq/g).

stratigraphical or foraminiferal evidence for subsidence in the northern section of the Palaeomagasa wetlands. Sediments at the Palaeomagasa site show foraminiferal assemblages consistent with gradual sediment accumulation and marsh development over the period of, and in the decades following, the earthquakes.

5. Discussion

5.1. Atalanti wetlands as recorders of earthquake subsidence

Based on biostratigraphical studies along the Cascadia margin, Nelson et al. (1996b) summarised the key criteria that permit coseismic subsidence to be distinguished from other non-seismic coastal processes. These criteria are: (1) the regional correlation of synchronous submergence; (2) evidence of sudden submergence; (3) a sizeable (metre-scale) amount of lasting submergence; (4) the coincidence of tsunami deposition with submergence; (5) the lateral continuity of peat–mud contacts across a wetland and between wetlands. In comparison to the Cascadia plate–boundary tectonic setting, the Aegean intra-plate normal faulting seismicity is an order of magnitude smaller. The influence of the earthquakes is consequently mainly concentrated in the epicentral zone. Therefore, the regional correlation of synchronous submergence is not applicable to the Atalanti area. Nevertheless, all four other criteria remain valid if wetlands of the type found in the Gulf of Atalanti are to be used as diagnostic indicators of earthquake-induced submergence.

Evidence of sudden submergence can be derived from the identification of abrupt vertical changes in microfossil assemblages or from sharp peaty soil/intertidal mud contacts (Nelson et al., 1996b). At both the Almyra and Gaïduronisi sites, sharp changes between sands/grits and clays show abrupt changes in depositional environment consistent with sudden subsidence. At a wetland site more distant from the fault (Palaomagasa), no stratigraphical or microfossil evidence for subsidence is detectable. At the Almyra site a marked biostratigraphical change from an intertidal to a shallow-marine environment around the time of the 1894 event is consistent with earthquake-

induced subsidence, but no reliable measure of the amount of subsidence is possible. The Gaïduronisi site shows the clearest evidence for sudden, lasting subsidence, with foraminiferal assemblages indicating an abrupt change from supratidal soil to intertidal marine conditions dated to the period of the earthquakes. The elevation change indicated by this terrestrial to marine transition is 30–80 cm. Immediately overlying the submerged soil in the Gaïduronisi core, the mixed marsh, intertidal and marine foraminifera within a thin sand unit, and the indication of rapid deposition (the absence of *R. globularis* with floating chambers), is consistent with tsunami deposition immediately following subsidence. Although thin sand units appear in many of the cores, however, the units cannot be correlated to a laterally extensive tsunami-deposited sand sheet. Similarly, the coastal stratigraphy in the Almyra-Skala Atalanti area lacks laterally extensive sharp soil–mud contacts of the type described in the Cascadia studies (Fig. 4). Hence, the key criteria summarised by Nelson et al. (1996b) that permit coseismic subsidence to be distinguished from other coastal processes are only partly fulfilled by these wetland sequences.

In the Aegean region sub-metre-scale coastal elevation changes are likely to be difficult to distinguish from the changes in sea level induced by other non-seismic processes (Table 1). The decimetre-scale subsidence estimated from the Gaïduronisi core is within the range that can be expected from shoreline adjustments to barrier breaching/migration or storm-surge flooding. In addition, the lack of laterally extensive sharp terrestrial–marine contacts (or tsunami deposits) means that earthquake-induced subsidence cannot be distinguished from barrier breaching/migration using spatial extent as a criterion (Table 1). Without well-defined, spatially traceable soil–mud couplets, reconstructing the pattern of wetland submergence across the study area is also problematic. In the present study, stratigraphical changes could be attributed to the 1894 earthquake rupture for only two reasons. Firstly, high-resolution dating control (^{210}Pb and ^{137}Cs) provided age estimates with a precision of ca. ±20 years. Secondly, the stratigraphical results could be compared directly with well-documented contemporary reports of the extent and magnitude of the observed coastal changes. For this reason, coastal wetland stratigraphies are only likely

Table 1
Amplitude, duration, permanence and length of coast affected by various types of rapid relative sea-level change in the Aegean (table format after Nelson et al., 1996b)

Process or type of change	Amplitude	Duration of change	Permanence of change	Length of coastline affected
Local tsunami	Up to 30 m[a]	Minutes	< 1 h	Tens to hundreds of kilometres
Storm surges	1 m[b]	Hours	Hours to days	Tens to hundreds of kilometres
Coseismic subsidence or uplift (moderate magnitude earthquakes)	0.3–0.8 m (this study) 1–3 m (Gulf of Corinth)[c]	Seconds	Centuries	Hundreds of metres–tens of kilometres
Semi-diurnal tides	0.6 m (Gulf of Evvia) Typically 0.1 m or less[d]	ca. 6 h	Hours	Entire Aegean region
Marine flooding from barrier breaching (natural or artificial coastal barriers)	Decimetres?[e]	Hours	Days to centuries	Hundreds of metres

[a] Maximum reported value for 1956 S. Aegean tsunami, Ambraseys (1960).
[b] Value for Z_{50} extreme sea-level, based on tide gauge records at N. Halkis, Gulf of Evvia (Tsimplis and Blackman, 1997).
[c] Based on estimates in Hubert et al. (1996) and Soter (1998).
[d] Zoi-Morou (1981).
[e] Depends on age of barrier, regional sea-level history, coastal morphology etc.

to be useful in identifying pre-historical or poorly documented earthquakes in the Aegean at sites where metre-scale coseismic elevation changes and/or major tsunami inundation have occurred.

5.2. Implications for tectonic models and earthquake-rupture scenarios for the Atalanti Fault

The stratigraphical results from the Atalanti wetlands support the idea of the coseismic submergence of the coast being between 30 and 80 cm. As a consequence, the contention that the rupture of the Atalanti Fault in the 1894 earthquake induced metre-scale (~1.5 m) subsidence of the coastal plain (Skuphos, 1894; Stiros and Rondoyianni, 1985; Stiros, 1986; Papazachos and Papazachou, 1997) is unlikely. However, as we illustrate below, using the coastal subsidence data presented here to test and refine tectonic models for the Atalanti fault is problematic.

Macroseismic maps by Philippson (1894) and Skuphos (1894) represent the 1894 rupture as a single fault trace extending from Skroponeri (10 km west of Chalkida) in the southeast to Kamena Vourla in the northwest (Fig. 8). It is this ~55-km-long rupture length that is reported by several modern earthquake catalogues (Karnik, 1968; Papazachos and Papazachou, 1997). However, the distribution of the surface

ruptures reported by Skuphos (1894) and subsequently mapped by Lemeille (1977) indicate firstly that the extent of the fault rupture is shorter than 55 km, and secondly that the existence of two separate lines of surface rupture could be the expression of two fault segments (Ambraseys and Jackson, 1990). In this regard, Roberts and Jackson (1991) defined the area between Kyparissi and Atalanti as being a step-over zone separating two fault segments (Fig. 1). Poulimenos and Doutsos (1996) and Ganas et al. (1998) also recognise these discrete structural segments, though Ganas et al. (1998) in particular argue that the 27 April 1894 earthquake ruptured through the intervening step-over zone, producing a single 34-km-long rupture. Each of these differing fault models ([1] a single >50-km-long fault; [2] a single 34-km-long fault, and [3] a ~34-km-long fault comprised of two segments) would produce contrasting patterns of vertical elevation changes across the epicentral area. A key question arising from this, therefore, is to what extent can the coastal elevation changes documented here help to evaluate which of these competing fault-rupture models is the more realistic?

To consider the significance of these contrasting structural schemes on the deformation pattern expected in the coastal region, we have used an elastic half-space dislocation model (Valensise and Ward, 1991) to simulate surface elevation changes induced
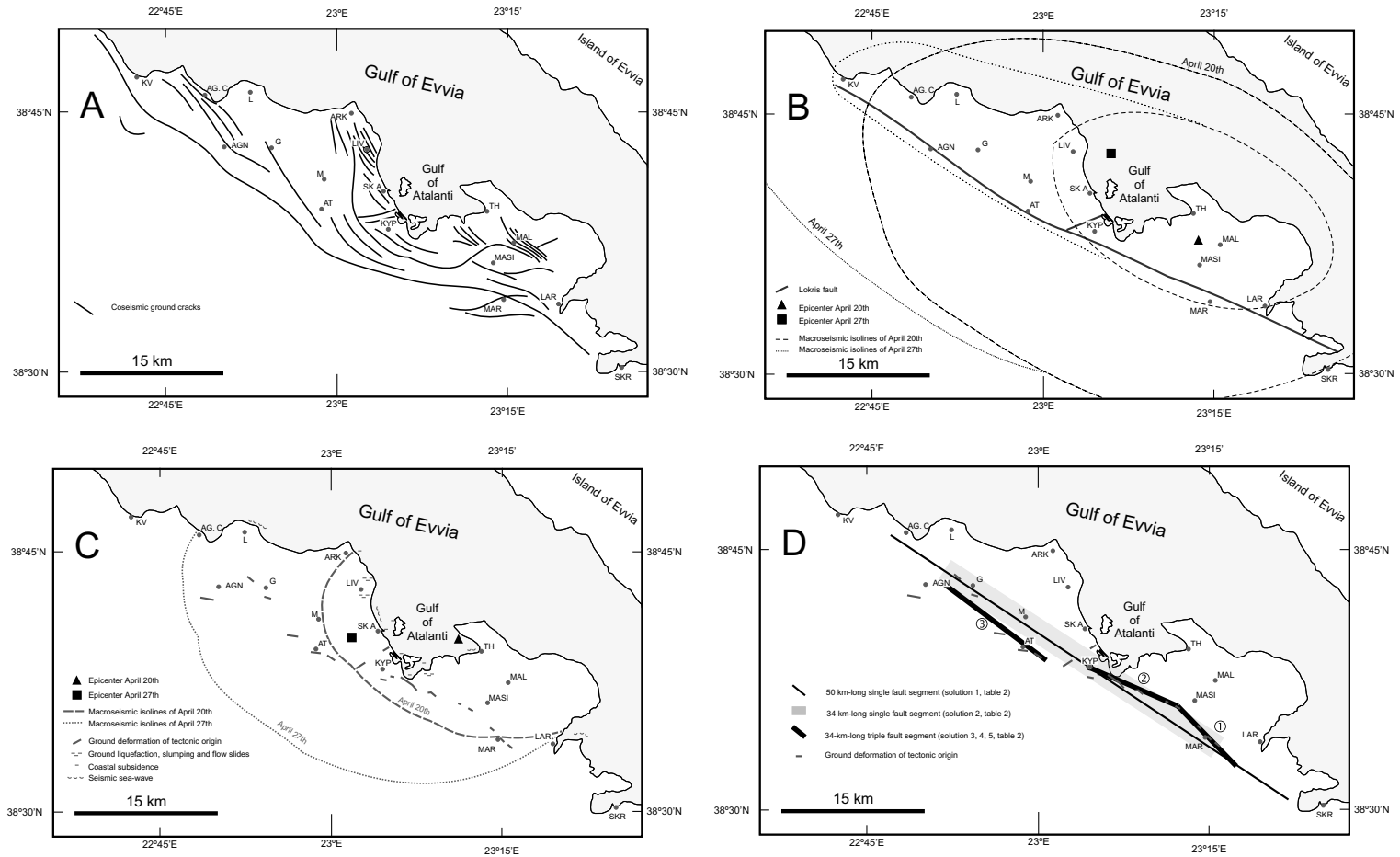
Fig. 8. General competing schemes of the 1894 Atalanti earthquake sequence. (A) Location of the ground breaks reported by Philippson, 1894 (redrawn from the original map). (B) General structure of the Atalanti (Lokris) seismogenic fault according to Skuphos, 1894. The dashed lines represent the isoseismals of both 20th and 27th of April seisms (redrawn from the original map). The epicenter locations are those given by Karnik (1968). (C) Ambraseys and Jackson's (1894) reinterpretation of the historical accounts reporting the effects of the earthquakes. The dashed lines represent the reinterpreted isoseismal. The locations of the epicentres, respectively a solid square and triangle, have been reassessed. (D) Possible scenario of the seismogenic fault structure. Solution 1 drawn as a thin black line refers to a 50-km-long fault. Solution 2 (grey rectangle) shows the 34-km-long fault segment of Ganas et al. (1998). Solution 3 (thick black line) presents a triple-fault-segment scenario which more closely fits the fault ruptures recognised by Lemeille (1977) and Ambraseys and Jackson (1990). The short dashes define the present-day ground deformation of tectonic origin recognised in the field. For more clarity see (C). KV: Kamena Vourla. AG C: Agios Constantinos. L: Longos. AGN: Agnandi. G: Goulemi. ARK: Arkitsa. LIV: Livanates. M: Megaplatanos. SKA: Skala Atalanti. A: Atalanti. KYP: Kyparissi. MASI: Masi. TH: Theologos. MAL: Malesina. LAR: Larymna. MAR: Martinon. SKR: Skroponeri.

by 1.5 m slip on: (1) a single 50-km-long fault; (2) a single 34-km-long fault; and (3) a 34-km-long fault comprised of two segments. The results are shown in Fig. 9 and in Table 2. The model of the 1894 Atalanti rupture as a single 50-km-long fault (Fig. 9a) predicts a large bowl of subsidence, with maximum subsidence being located in the middle of the fault segment, i.e. at Kyparissi. The simulation of slip on the 34-km-long fault illustrates how decreasing the fault length results only in a reduction in the along-strike extent of deformation; the width and pattern of the deformation zone remains virtually unchanged (Fig. 9b). The general pattern of deformation, however, is dramatically altered if the fault is subdivided into two segments (Fig. 9c). With a two-segment fault model, a saddle of relatively minor subsidence (~10 cm) occurs in the step-over area at Kyparissi, precisely the area where subsidence was greatest (~60 cm) in the single fault model. The possibility that the slip of the fault was

smaller (i.e. 1 m, Ambraseys and Jackson, 1998) has also been examined (Table 2, Fig. 9d). It appears that the area affected by the deformation remains identical, and only the magnitude of the uplift and subsidence is affected.

When the stratigraphical data are considered, at Almyra the identification of a sudden deepening from intertidal to a shallow marine depositional conditions does not constrain the amount of subsidence. For this site, the biostratigraphical evidence is unable to discriminate between the modelled subsidence estimate range of 0.36–0.89 m (Table 2). At Palaeomagasa, the absence of detectable subsidence is difficult to reconcile with the upper subsidence estimates of around 0.6 m expected from the single segment fault models (1 and 3, Table 2); the lower subsidence values of 0.25–0.37 m predicted by the multi-segment model as well as the 0.37–0.40 m of the single segment with 1 m slip (2 and 4, Table 2),

Table 2

Fault parameters input for modelling the dislocation pattern triggered by the 1894 Atalanti earthquake sequence according to the expected deformation of an elastic half-space (Valensise and Ward, 1991).

Segments (1)–(3) are the fault segments described in Fig. 8D. Segment (1) is the southernmost segment located around Martinon (MAR Fig. 8), the second segment (2) ends around Kyparissi (KYP Fig. 8) while the last segment (3) spreads across the area of Atalanti towards Agnandi and Goulemi (respectively, AT, AGN and G Fig. 8). The length of both first segments (1) and (2) is deduced from the topography and the surface ruptures (Lemeille, 1977; Ambraseys and Jackson, 1990). The length of the last segment (3) is given by Ambraseys and Jackson (1990). The *depth of the top* of the fault is the depth at which the fault plane ends towards the surface. This is a requirement of elastic modelling where the break never reaches the surface. In this case, this parameter has been set by using the electric profiles of the Atalanti plain presented in Ganas et al. (1998, Fig. 9)

Single segment model					Multi-segment model			
Constant parameters					*Constant parameters for each segment*			
						Segment (1)	Segment (2)	Segment (3)
Width downdip (km)	10				Length (km)	8.9	10.6	15[a]
Depth of the top (m)	500				Depth of the top (m)	500[b]	300[b]	600[b]
Azimuth (N°E)	290				Azimuth (N°E)	315	292	317
Dip (°)	55				*Constant common parameters*			
Rake (°)	290[a]				Width downdip (km)		10	
					Dip (°)		55	
					Rake (°)		290[a]	
	Solution 1	Solution 2	Solution 3	Solution 4		Solution 5	Solution 6	
Length (km)	50		34[b]					
Slip (m)	1.5[c]	1[a]	1.5[c]	1[a]	Slip (m)	1.5[c]	1[a]	
Expected local deformation (m)					*Expected local deformation (m)*			
Almyra site	−0.89	−0.60	−0.54	−0.36	Almyra site	−0.70	−0.46	
Gaïduronisi site	−0.75	−0.50	−0.86	−0.57	Gaïduronisi site	−0.82	−0.54	
Palaeomagasa site	−0.59	−0.40	−0.65	−0.36	Palaeomagasa site	−0.37	−0.25	

[a] Ambraseys and Jackson, 1998.
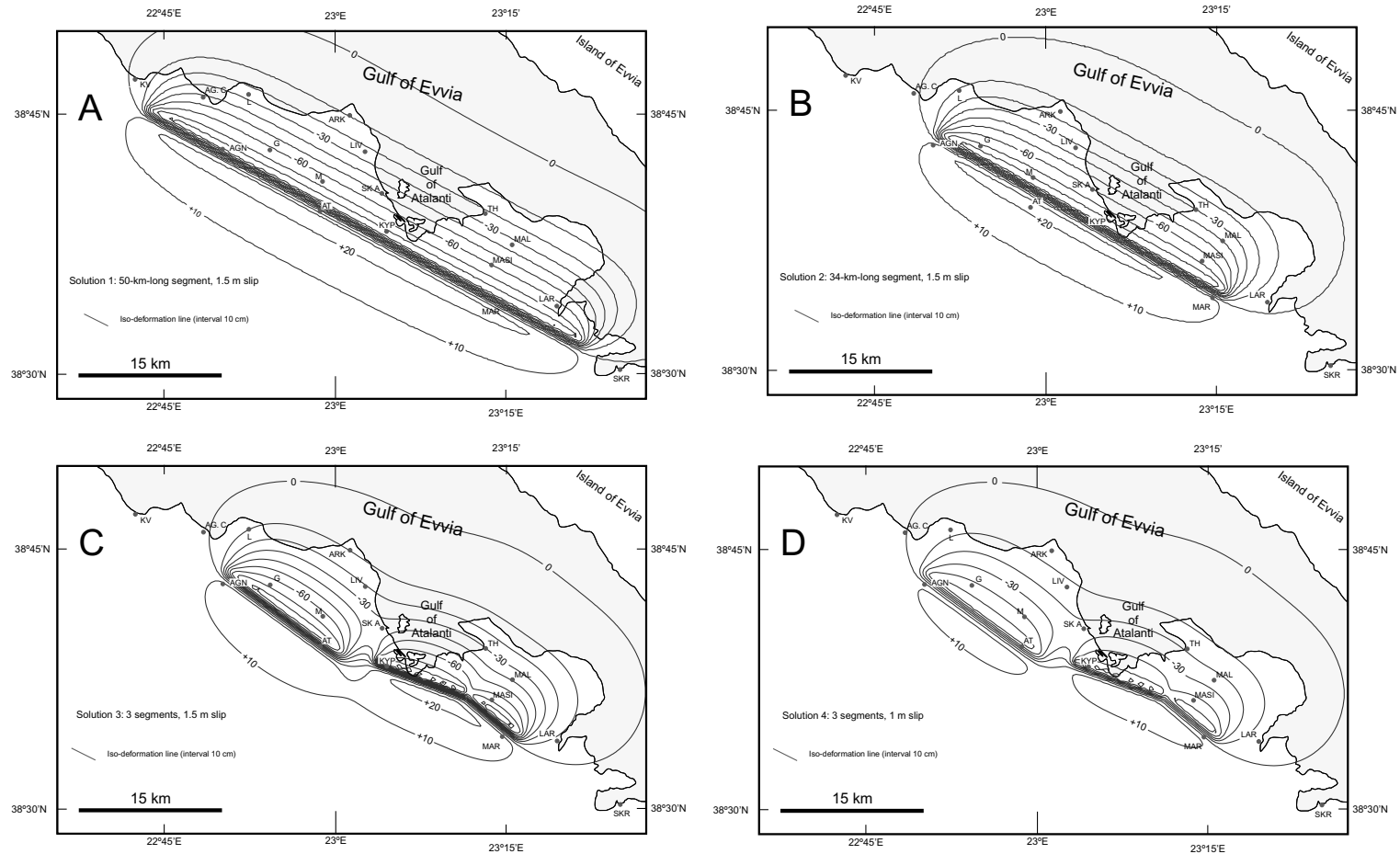[b] Ganas et al., 1998.
[c] Papazachos and Papazachou, 1997.

Fig. 9. Modelling of the earthquakes' pattern of deformation according to the expected deformation of an elastic half-space under a normal faulting process (Valensise and Ward, 1991). The lines represent the 10 cm contour lines of equal deformation of the ground. We present three types of potential scenario of rupture. All three models assume a slip of 1.5 m on a 55°-north-dipping fault plane with a rake of 290° (normal faulting with a slight left lateral component, see Table 2 for details on the fault parameters). (A) reports a 50-km-long single fault pattern of dislocation. This solution is close to that retained in historical catalogues (Papazachos and Papazachou, 1997). (B) sketches the 34-km-long rupture suggested by Ganas et al. (1998). The area affected by the alongstrike deformation is variable from one model to the other, however the magnitude of the vertical displacement perpendicularly to the fault is virtually identical whatever the length of the incriminated fault. (C) proposes a triple fault segment interpretation of the rupture as evoked by Roberts and Jackson (1991). The pattern of deformation is significantly different in the area between Kyparissi and Atalanti (KYP and AT) where a ridge of relatively limited subsidence appears. At Skala Atalanti (SKA) the subsidence diminishes from −60 cm to −35 cm. (D) is the most favoured scenario. The three segments model is retained, but the slip is only of 1 m which is more in accordance with the subsidence estimate derived from the Gaïduronisi site. KV: Kamena Vourla. AG C: Agios Constantinos. L: Longos. AGN: Agnandi. G: Goulemi. ARK: Arkitsa. LIV: Livanates. M: Megaplatanos. SKA: Skala Atalanti. A: Atalanti. KYP: Kyparissi. MASI: Masi. TH: Theologos. MAL: Malesina. LAR: Larymna. MAR: Martinon. SKR: Skroponeri.

however, are within the range of uncertainty of the biostratigraphical data. At Gaïduronisi, the observed possible range of subsidence of 0.3–0.8 m is equivalent to the range of expected subsidence values produced by all the models (Table 2). Overall, the observed coastal stratigraphical data are unable to unequivocally support one model to the exclusion of the others. However, in general, the various lines of evidence would suggest that the observed coastal elevation changes are best accounted for by a 1 m slip dislocation on a multi-segment fault.

Similarities in the subsidence estimates predicted by the competing models indicate that further stratigraphical studies in the Atalanti wetlands are unlikely to significantly refine the optimum fault model. The resolution of the biostratigraphical data and radiometric dating is unable to discriminate between the comparatively minor elevation changes predicted for the central portion of the Atalanti wetlands (around Gaïduronisi). Improved subsidence estimates in the northern portion of the wetlands, in the vicinity of Palaeomagasa, may help to constrain the models further. However, it is important to note that, by comparison, adjustments to key fault parameters, particularly the location and geometry of the fault plane, will have a considerably greater effect on the pattern and magnitude of deformation models. These parameters are still poorly documented for the Atalanti Fault, and further geological studies need to verify the segmented nature of this structure. Furthermore, the models present only coseismic elevation changes but the coastal stratigraphy records the net effects of coseismic and postseismic displacement, and also of possible sediment compaction. In summary, we conclude that the resolution of the coastal stratigraphical data is too coarse to realistically disentangle all these variables, and thus can only be used in a general sense to elucidate tectonic models.

Although coastal wetland stratigraphies are of only limited value in refining the tectonic models for the 1894 Atalanti earthquakes, they can provide some insights on past earthquake activity inferred on the Atalanti Fault. While the stratigraphical expression of the coseismic subsidence induced by the 1894 Atalanti earthquakes is subtle, the morphologic and hydrodynamic changes to the Gulf of Atalanti coastline were dramatic. The most notable of these modifications, the separation of the Gaïduronisi peninsula

from the mainland, was possible only because the decimetre-scale subsidence was sufficient to induce widespread inundation of the low-lying coastal marshes. Skuphos (1894) was the first to note the similarity between the detachment of Gaïduronisi island during the 1894 earthquakes and literary accounts of the formation of nearby Atalanti Island during the destructive earthquake of 426 BC (see also Guidoboni et al., 1989). Recent studies (e.g. Stiros and Dakoronia, 1989) have argued that the reported formation of Atalanti Island and the associated marine inundation around the Gulf of Atalanti during the 426 BC event indicate that the earthquake was caused by rupture along the Atalanti Fault, producing tectonic subsidence and tsunami inundation in the same manner as in 1894. The data presented here indicate that the 1894 earthquake-induced coastal changes provide a misleading analogy for the 426 BC earthquake. In contrast to the few hundreds of metres width of low-gradient wetland strip that separates Gaïduronisi Island from the mainland, the coastal bathymetry shows that Atalanti Island is separated by an 11-m-deep marine channel. Generating this offshore topography by coseismic subsidence in the hangingwall of the Atalanti Fault is difficult to conceive. Maximum tectonic subsidence is expected close to the Atalanti Fault, and should be reduced considerably at distances of 3.5 km from the fault. Palaeomagasa, the wetland site closest to Atalanti Island, shows no stratigraphical evidence for appreciable subsidence in the 1894 earthquake. Even assuming a rupture of the whole length (50–60 km) of the Atalanti Fault, only 50–60 cm of subsidence would be expected in the vicinity of Atalanti Island for a 1.5 m-slip, rather than the several metres that are required for its detachment. To the northwest of Atalanti Island, at Kynos (Fig. 1), shoreline features that are dated broadly contemporaneous with the 426 BC event occur at elevations of around a metre above sea level (Pirazzoli et al., 1999). This indicates the probable tendency for the coastline north of Skala Atalanti to be uplifted in the footwall of the Kamena Vourla Fault (Roberts and Jackson, 1991). Atalanti Island appears, therefore, to be located in the transfer zone between two seismogenic normal faults, where alternating increments

of minor seismic subsidence and uplift would be expected to counterbalance each other. In summary, the geomorphological and stratigraphical evidence reinforces the assessment of the literary and archaeological evidence by Buck and Stewart (2000) that the 426 BC earthquake was unlikely to have been generated by rupture on the Atalanti Fault.

6. Conclusions

The 1894 earthquake sequence in the Gulf of Atalanti caused significant shoreline changes, particularly the separation of the Gaïduronisi peninsula from the mainland. Coastal wetland stratigraphies in the Gaïduronisi area show evidence for sudden, lasting subsidence contemporaneous with the 1894 events, with foraminiferal assemblages at a site on the mainland opposite the island indicating an abrupt change from supratidal soil to intertidal marine conditions. The elevation change indicated by this terrestrial to marine transition is 30–80 cm. The coastal stratigraphy in the Atalanti area however lacks laterally extensive sharp soil–mud contacts or tsunami deposits of the type used in identifying past earthquake subsidence events at plate–boundary settings. Despite major changes in coastal configuration, the stratigraphical signature of the 1894 earthquakes is relatively subtle, and is consequently difficult to distinguish from other rapid coastal changes (e.g. storm events or barrier breaching) without high-resolution dating control and reference to documentary records. In addition, the resolution of the biostratigraphic data reported here is insufficient to distinguish between the contrasting fault rupture models for the 1894 events. The coastal elevation changes recorded in these wetlands, however, are best accounted for by a slip of 1 m on a multi-segment fault.

Acknowledgements

References

Akropolis newspaper, 1894. 10th April–21st April, Athens. (In Greek.)

Ambraseys, N.N., 1960. The seismic sea wave of July 9th 1956 in the Greek archipelago. J. Geophys. Res. 65, 1257–1265.

Ambraseys, N.N., Jackson, J.A., 1990. Seismicity and associated strain of central Greece between 1890 and 1988. Geophys. J. Int. 101, 663–708.

Ambraseys, N.N., Jackson, J.A., 1998. Faulting associated with historical and recent earthquakes in the Eastern Mediterranean region. Geophys. J. Int. 133, 390–406.

Appleby, P.G., Oldfield, F., 1992. Applications of ^{210}Pb to sedimentation studies. In: Ivanovich, M., Harmon, R.S. (Eds.). Uranium-series disequilibrium. Applications to Earth, Marine and Environmental Sciences, 2nd ed.. Oxford Science, Oxford.

Atwater, B.F., Nelson, A.R., Clague, J.J., Carver, G.A., Yamaguchi, D.K., Bobrowsky, P.T., Borgeois, J., Darienzo, M.E., Grant, W.C., Hemphill-Haley, E., Kelsey, H.M., Jacoby, G.C., Nishenko, S.P., Palmer, S.P., Peterson, C.D., 1995. Summary of coastal geologic evidence for great earthquakes at the Cascadia subduction zone. Earthquake Spectra 11, 1–18.

Bennett, K.D., Whittington, G., Edwards, K.J., 1994. Recent plant nomenclatural changes and pollen morphology in the British Isles. Quaternary Newsletter 73, 1–6.

Buck, V., Stewart, I., 2000. A critical appraisal of the Classical texts and Archaeological evidence for classical earthquakes in the Atalanti Region, central mainland Greece. In: McGuire, W.J., Griffiths, D., Hancock, P.L., Stewart, I.S. (Eds.). The Archaeology of Geological Catastrophes, Geological Society, London, Special Publications, 171, 33–44.

Cimerman, F., Langer, M.R., 1991. Mediterranean Foraminifera. Slovenska akademija znanosti in umetnosti, Ljubljana.

Clague, J.J., Bobrowsky, P.T., 1994. Evidence for a large earthquake and tsunami 100–400 years ago on western Vancouver Island, British Columbia. Quat. Res. 41, 176–184.

Cundy, A.B., Croudace, I.W., 1996. Sediment accretion and recent sea-level rise in the Solent, southern England: inferences from radiometric and geochemical studies. Estuar., Coast. Shelf Sci. 43, 449–467.

Cundy, A.B., Collins, P.E.F., Turner, S.D., Croudace, I.W., Horne, D., 1998. 100 years of environmental change in a coastal wetland, Augusta Bay, southeast Sicily: evidence from geochemical and palaeoecological studies. In: Black, K.S., Paterson, D.M., Cramp, A. (Eds.). Sedimentary Processes in the Intertidal Zone, Geological Society, London, Special Publications, vol. 139. Geological Society, pp. 243–254.

Darienzo, M.E., Peterson, C.D., Clough, C., 1994. Stratigraphical evidence for great subduction-zone earthquakes at four estuaries in northern Orego, USA. J. Coast. Res. 10, 850–876.

Donnici, S., Barbero, R.S., Taroni, G., 1997. Living benthic foraminifera in the Lagoon of Venice (Italy): population dynamics and its significance. Micropalaeontology 43, 440–454.

Flynn, W.W., 1968. Determination of low levels of ^{210}Po in environmental materials. Anal. Chim. Acta 43, 221–227.

Ganas, A., Roberts, G.P., Memou, T.Z., 1998. Segment boundaries, the 1894 ruptures and strain patterns along the Atalanti Fault Segment, central Greece. J. Geodynamics 26, 461–486.

Gawthorpe, R.L., Hurst, J.M., 1993. Transfer zones in extensional basins: their structural style and influence on drainage development and stratigraphy. J. Geol. Soc. Lond. 150, 1137–1152.

Gehrels, W.R., Leatherman, S.P., 1980. Sea-level rise — animator and terminator of coastal marshes: an annotated bibliography on US coastal marshes and sea-level rise. Vance bibliographies, Pub. Admin. Series: Bibliography, p. 2634.

Goldberg, E.D., 1963. Geochronology with ^{210}Pb in radioactive dating. IAEA, Vienna, pp. 121–131.

Guidoboni, E., Comastri, A., Traina, G., 1989. Catalogue of ancient earthquakes in the Mediterranean area up to the 10th century. Editrice Compositori, Rome.

Guilbault, J.-P., Clague, J.J., Lapointe, M., 1995. Amount of subsidence during a late Holocene earthquake — evidence from fossil tidal marsh foraminifera at Vancouver Island, west coast of Canada. Palaeo., Palaeo., Palaeo. 118, 49–71.

Hemphill-Haley, E., 1995. Diatom evidence for earthquake-induced subsidence and tsunami 300 yr ago in southern coastal Washington. Geol. Soc. Am. Bull. 107, 367–378.

Hubert, A., King, G., Armijo, R., Meyer, B., Papanastassiou, D., 1996. Fault reactivation, stress interaction and rupture propagation of the 1981 Corinth earthquake sequence. Earth Planet. Sci. Lett. 142, 573–585.

Jones, R.W., 1994. The Challenger Foraminifera, Oxford Science Publications, The Natural History Museum, London.

Karnik, V., 1968. Seismicity of the European Area, Academia Publishing House, Prague.

Lemeille, F., 1977. Etudes néotectoniques en Grèce centrale nord-orientale: Eubée centrale, Attique, Béotie, Locride et dans les Sporades du Nord, (Skiros), Thesis, Université de Paris-Sud Orsay.

Long, A.J., Shennan, I., 1994. Sea-Level Changes in Washington and Oregon and the 'Earthquake Deformation Cycle'. J. Coast. Res. 10, 825–838.

Mathewes, R.W., Clague, J.J., 1994. Detection of large prehistoric earthquakes in the Pacific-northwest by microfossil analysis. Science 264, 688–691.

McNeill, L.C., Goldfinger, C., Yeats, R.S., Kulm, L.D., 1998. The effects of upper plate deformation on records of prehistoric Cascadia subduction zone earthquakes. In: Stewart, I.S., Vita-Finzi, C. (Eds.). Coastal Tectonics, Geological Society, Special Publications, vol. 146. Geological Society, London, pp. 319–340.

Mitsopoulos, K., 1895. The Lokris mega-earthquake, 40p, Athens. (In Greek.).

Moore, P.D., Webb, J.A., Collinson, M.E., 1991. Pollen Analysis, 2nd ed. Blackwell Scientific, Oxford.

Muir Wood, R., King, G.C.P., 1993. Hydrological signatures of earthquake strain. J. Geophys. Res. 98 (B12), 22 035–22 068.

Nelson, S.N., Jennings, A.E., Kashima, K., 1996a. An earthquake history derived from the stratigraphical and microfossil evidence of relative sea-level change at Coos Bay, southern coastal Oregon. Geol. Soc. Am. Bull. 108, 141–154.

Nelson, A.R., Shennan, I., Long, A.J., 1996b. Identifying coseismic subsidence in tidal-wetland stratigraphical sequences at the Cascadia subduction zone of western North America. J. Geophys. Res. 101 (B3), 6115–6135.

Papavasiliou, M.S.A., 1894. On the earthquakes of Lokris (Greece) April 1894. Compte rendu de l'Acad. des Sci. de Paris, T. CXIX:1.

Papazachos, B., Papazachou, C., 1997. The Earthquakes of Greece, Ziti Editions, Thessaloniki (304p).

Pavlides, S., Caputo, R., Chatzipetros, A., 1998. Empirical relationships among earthquake magnitude, surface ruptures and maximum displacement in the broader Aegean region. Proceedings of the Third International Conference on the Geology of the Eastern Mediterranean. (ICGEM3), Nicosia-Cyprus (in press).

Philippson, A., 1894. Das diesjahrige Erdbeben in Lokris. Verhandlungen der Geselschaft fur Erdkunde zu Berlin, vol. 21, 3p.

Pirazzoli, P.A., Stiros, S.C., Arnold, M., Laborel, J., Laborel-Deguen, F., 1999. Late Holocene coseismic vertical displacements and tsunami deposits near Kynos, Gulf of Euboea, central Greece. Phys. Chem. Earth 24, 361–367.

Poulimenos, G., Doutsos, T., 1996. Barriers on seismogenic faults in Greece. J. Geodynamics 22, 119–136.

Ritchie, J.C., McHenry, J.R., 1990. Application of radioactive fallout caesium-137 for measuring soil erosion and sediment accumulation rates and patterns: a review. J. Environ. Quality 19, 215–233.

Roberts, S., Jackson, J., 1991. Active normal faulting in central Greece: an overview. In: Roberts, A.M., Yielding, G., Freeman, B. (Eds.). The Geometry of Normal Faults, Geological Society, Special Publications, 56. Geological Society, London, pp. 125–142.

Rondoyianni-Tsiambaou, Th., 1984. Etude Néotectonique des rivages occidentaux du Canal d'Atalanti (Grèce Centrale), Doctoral Dissertation, Univ. de Paris Sud, 200p.

Scott, D.B., Medioli, F.S., 1978. Vertical zonations of marsh foraminifera as accurate indicators of former sea level. Nature 272, 528–531.

Scott, D.B., Piper, D.J.W., Panagos, A.G., 1979. Recent salt marsh and intertidal mudflat foraminifera from the western coast of Greece. Riv. Ital. Paleont. 85, 243–265.

Shennan, I., Long, A.J., Rutherford, M.M., Green, F.M., Innes, J.B., Lloyd, J.M., Zong, Y., Walker, K.J., 1996. Tidal-marsh stratigraphy, sea-level change and large earthquakes, I: a 5000 year record in Washington, USA. Quat. Sci. Rev. 15, 1023–1059.

Shennan, I., Long, A.J., Rutherford, M.M., Innes, J.B., Green, F.M., Kirby, J.R., Walker, K.J., 1998. Tidal-marsh stratigraphy, sea-level change and large earthquakes, II: Submergence events during the last 3500 years at Netarts Bay, Oregon, USA. Quat. Sci. Rev. 17, 365–393.

Skuphos, T., 1894. Die zwei grossen Erdbeben in Lokris am 8/20 und 15/27 April 1894. Zeitschrift Ges. Erdkunde zu Berlin, vol. 24, pp. 409–474.

Smith, F.B., 1988. Lessons from the dispersion and deposition of debris from Chernobyl. Meteorol. Mag. 117, 310–317.

Soter, S., 1998. Holocene uplift and subsidence in the Helike Delta, Gulf of Corinth, Greece. In: Stewart, I.S., Vita-Finzi, C. (Eds.). Coastal Tectonics, Geological Society, Special Publications, vol. 146. Geological Society, London, pp. 41–56.

Stiros, S., Dakoronia, P., 1989. Rulo Storico e Identificazione di Antichi Terremoti nei siti della Grecia. In: Guidoboni, E. (Ed.). I Terremoti Prima del Mille in Italia e nell' area Mediterranea, SGA Storia-Geofisica-Ambiente, Bologna, pp. 422–438.

Stiros, S.C., 1986. Geodetically controlled taphrogenesis in back-arc environments: three examples from central and northern Greece. Tectonophysics 130, 281–288.

Stiros, S.C., Rondoyianni, T., 1985. Recent vertical movements across the Atalanti Fault-Zone (Central Greece). Pageoph. 123, 837–848.

Tsimplis, M.N., Blackman, D., 1997. Extreme sea-level distribution and return periods in the Aegean and Ionian Seas. Estuar., Coast. Shelf Sci. 44, 79–89.

Zoi-Morou, A., 1981. Tide-gauge data of Hellenic harbours. Ocean. Stud. Hydrog. Surv. Athens 13.